Translational Oncology
www.transonc.com

Volume 12 Number 7 July 2019 pp. 895–907 895

Chemically Modified Variants of Fenofibrate with Antiglioblastoma Potential[1,2]

J. Stalinska[*,†,‡,¶], E. Zimolag[*,†,‡], NA. Pianovich[#], A. Zapata[*,†,‡], A. Lassak[*,†,‡], M. Rak[¶], M. Dean[†,‡], D. Ucar-Bilyeu[†,‡], D. Wyczechowska[†,‡], F. Culicchia[‡], L. Marrero[‡,§], L. Del Valle[*,†,‡], J. Sarkaria[††], F. Peruzzi[*,†,‡], BS Jursic[#,**] and K. Reiss[*,†,‡]

[*]Neurological Cancer Research, LSU Health Sciences Center, New Orleans, LA; [†]Stanley S. Scott Cancer Center at LSU Health Sciences Center, New Orleans, LA; [‡]School of Medicine, LSU Health Sciences Center, New Orleans, LA; [§]Department of Orthopedic Surgery, LSU Health Sciences Center, New Orleans, LA; [¶]Department of Cell Biology, Faculty of Biochemistry, Biophysics and Biotechnology, Jagiellonian University, Cracow, Poland; [#]Department of Chemistry, University of New Orleans, New Orleans, LA; [**]Stepharm LLC, P.O. Box 24220, New Orleans, LA; [††]Department of Radiation Oncology, Mayo Clinic, Rochester, Minnesota, MN

Abstract

Anticancer effects of a common lipid-lowering drug, fenofibrate, have been described in the literature for a quite some time; however, fenofibrate has not been used as a direct anticancer therapy. We have previously reported that fenofibrate in its unprocessed form (ester) accumulates in the mitochondria, inhibits mitochondrial respiration, and triggers a severe energy deficit and extensive glioblastoma cell death. However, fenofibrate does not cross the blood brain barrier and is quickly processed by blood and tissue esterases to form the PPARα agonist fenofibric acid, which is practically ineffective effective in triggering cancer cell death. To address these issues, we have made several chemical modifications in fenofibrate structure to increase its stability, water solubility, tissue penetration, and ultimately anticancer potential. Our data show that, in comparison to fenofibrate, four new compounds designated here as PP1, PP2, PP3, and PP4 have improved anticancer activity *in vitro*. Like fenofibrate, the compounds block mitochondrial respiration and trigger massive glioblastoma cell death *in vitro*. In addition, one of the lead compounds, PP1, has improved water solubility and is significantly more stable when exposed to human blood in comparison to fenofibrate. Importantly, mice bearing large intracranial glioblastoma tumors demonstrated extensive areas of tumor cell death within the tumor mass following oral administration of PP1, and the treated mice did not show any major signs of distress, and accumulated PP1 at therapeutically relevant concentrations in several tissues, including brain and intracranial tumors.

Translational Oncology (2019) 12, 895–907

Address all correspondence to: Krzysztof Reiss, Neurological Cancer Research, Stanley S Scott Cancer Center, Louisiana State University Health Sciences Center, 1700 Tulane Ave., New Orleans, LA 70112. E-mail: kreiss@lsuhsc.edu

[1] Financial support: This work was supported by LSUHSC, Dean of School of Medicine matching funds (K.R.); and P20-GM121288-01 (K.R.).

[2] Disclosure of potential conflict of interest: Dr. Branko Jursic is an employee of Stepharm LLC, P.O. Box 24220, New Orleans, LA; Dr. Krzysztof Reiss and Dr. Branko Jursic applied for LSU provisional patent for the described PP compounds. Other authors do not have any financial interest in relation to this submission.

Received 15 January 2019; Revised 8 April 2019; Accepted 10 April 2019

1936-5233/19
https://doi.org/10.1016/j.tranon.2019.04.006

Introduction

Glioblastomas are highly lethal brain tumors for which therapeutic options are limited. Rapidly growing and highly invasive glioblastoma cells rely on both glycolysis and mitochondrial respiration to generate sufficient amounts of ATP and intermediate metabolites (anaplerosis). Interfering with these pathways may be a promising therapeutic strategy to induce "metabolic catastrophe" in these practically incurable brain neoplasms. We have demonstrated that tumor cells of neuroectodermal origin, including melanoma, medulloblastoma, and glioblastoma, are highly sensitive to the metabolic drug fenofibrate (FF) [1–11]. FF is routinely used as a lipid-lowering drug through the ability of its metabolite, fenofibric acid (FA), to activate peroxisome proliferator activated receptor alpha (PPARα) [12]. Although activation of PPARα may explain some of the observed anticancer effects, glioblastoma cells treated with PPARα siRNA retain sensitivity to FF, indicating a PPARα-independent mechanism of its anticancer action. Indeed, our previously published data demonstrate that unprocessed FF (ester) accumulates in mitochondrial membranes, with evidence that mitochondrial FF triggers a severe and immediate inhibition of mitochondrial respiration. This leads to a severe decline in intracellular ATP, and apoptotic tumor cell death [11]. We also reported that FF is promptly processed to FA by blood and tissue esterases, and FA is much less effective in triggering tumor cell death, and that both FF and FA do not cross the blood brain tumor barrier (BBTB) [4]. To address these issues, which are hampering development of more effective FF-based antitumoral therapies, we have made several chemical modifications to improve FF stability, water solubility, tissue penetration, and ultimatelly antiglioblastoma efficacy. Our data show that, in comparison to FF, four compounds, designated as PP1, PP2, PP3, and PP4, have improved cytotoxicity against glioblastoma cells *in vitro*; similar to FF, they block mitochondrial respiration. In addition, PP1 is significantly more stable when exposed to human blood and has improved water solubility. We have also demonstrated that mice treated with PP1 (oral administration) accumulated PP1 at therapeutically relevant concentrations in several tissues including intracranial glioblastoma tumors and survived the treatment without any major signs of distress. Importantly, mice with large intracranial glioblastomas demonstrated extensive areas of necrosis, which were detected exclusively in PP1-treated mice, further supporting a strong antiglioblastoma potential of this new metabolic compound.

Materials and Methods

Chemical Procedures to Prepare PP Compounds

All starting materials were reagent grade purchased from Sigma-Aldrich or Ark Pharm. ^{1}H-NMR spectra were recorded on Varian Mercury Plus 400-MHz instrument in $CDCl_3$ or DMSO-d_6, with the solvent chemical shifts as an internal standard. All computed molecular descriptors were generated by Chemaxon MarvinSketch version 18.8.0.

Preparation of 2-[4-(4-Chlorobenzoyl)phenoxy]-N-(2-hydroxyethyl)-N,2-dimethylpropanamide (PP1). Method A: Dichloromethane (20 ml) suspension of FA (318.75 mg; 1 mmol) and oxalyl chloride (0.25 mL; 380.1 mg; 3 mmol), and one drop of *N,N*-dimethylformamide were stirred at room temperature for 5 hours. Solvent was evaporated under reduced pressure. White solid residue was resolved in in dichloromethane (10 ml) and again evaporated to the solid residue. This solid residue was dissolved in dichloromethane (20 ml), and at room temperature with stirring, dichloromethane (10 ml) solution of 2-(methylamino)ethanol (0.24 ml; 225 mg; 3 mmol) was gradually added. Reaction mixture was stirred at room temperature. Dichloromethane reaction mixture was washed with water (3×15 ml), 5% hydrochloric acid (3×15 ml), water (3×15 ml), 10% sodium carbonate (3×15 ml), and finally water (3×15 ml) and dried over anhydrous sodium carbonate. Solvent was evaporated under reduced pressure to result in a viscous pale-yellow liquid (390 mg). Product was crystalized from dichloromethane/hexane (30 ml; 1:4) at room temperature by slow solvent evaporation to 1/5 original volume, and formed crystals were washed with ice-cold hexane. Isolated yield 340 mg (90%).

Method B: Dichloromethane (100 ml) solution of FA (637 mg; 2 mmol), 1-ethyl-3-(3-dimethylaminopropyl)carbodiimide, hydrochloride (EDC, 576; 3 mmol), and 2-(methylamino)ethanol (600 mg; 8 mmol) was stirred at room temperature overnight. Dichloromethane solution was washed with 5% hydrochloric acid (5×20 ml), water (5×20 ml), 10% sodium carbonate (5×20 ml), and water (3×20 ml) and dried over anhydrous sodium carbonate. After solvent evaporation, oily residue was crystalized from dichloromethane/hexane (1:4) to give pure product (640 mg; 85% yield). ^{1}H-NMR ($CDCl_3$) δ 7.74 (2H, δ, J = 8.8 Hz), 7.71 (2H, d, J = 8.8 Hz), 7.45 (2H, d, J = 8.8 Hz), 6.92 (2H, d, J = 8.8 Hz), 3.78 (2H, t, J = 4.8 Hz), 3.53 (2H, t, J = 4.8 Hz), 3.6 (1H, broad s), 3,17 (3H, s), and 1.71 (6H, s) ppm. ^{13}C-NMR ($CDCl_3$) δ 194.1, 173.5, 159.3, 138.3, 136.1, 132.2, 131.1, 130.3, 128.5, 116.5, 81.4, 60.3, 52.8, 36.7, and 25.7 ppm.

Preparation of 2-[4-(4-Chlorobenzoyl)phenoxy]-2-methyl-1-(4-methylpiperazin-1-yl)propan-1-one (PP2). Dichloromethane (30 ml) of fenofibric chloride (1 mmol; prepared as described above for **PP1** preparation) was slowly added in stirring water (5 ml) solution of sodium carbonate (216 mg; 2 mmol) with tetrahydrofuran (10 ml) and of 1-methylpiperazine (0.13 ml; 120 mg; 1.2 mmol). Resulting reaction mixture was stirred at room temperature for 1 hour. Additional water (30 ml) was added, and the organic layer was separated; washed with water (3×10 ml), 5% hydrochloric acid (3x10 ml), 10% sodium carbonate (3x10 ml), and water; and dried over anhydrous sodium carbonate. After evaporation, oily residue was crystalized from dichloromethane hexane to give 350 mg (88%) of pure product. ^{1}H-NMR (DMSO-d_6) δ 7.71 (2H, d, J = 8.8 Hz), 7.67 (2H, d, J = 8.8 Hz), 7.58 (2H, d, J = 8.4 Hz), 6.90 (2H, d, J = 8.4 Hz), 3.64 (2H, broad s), 3.46 (2H, broad s), 2.12 (2H, broad s), 1.98 (3H, s), and 1.59 (6H, s) ppm. ^{13}C-NMR (DMSO-d_6) δ 193.6, 169.0, 159.5, 137.6, 136.6, 132.5, 131.6, 130.1, 129.1, 116.8, 81.7, 54.7, 45.9, 42.9, and 26.1 ppm.

Preparation of 2-[4-(4-Chlorobenzoyl)phenoxy]-N,2-dimethyl-N-[(2S,3R,4R,5R)-2,3,4,5,6-pentahydroxyhexyl]propenamide (PP3). FA chloride prepared from FA (318.75 mg; 1 mmol) and oxalyl chloride (0.25 mL; 380.1 mg; 3 mmol) as described for preparation of PP1 was dissolved in dichloromethane (15 ml) and mixed with acetonitrile (20 ml) and water (10 ml) solution of *N*-methyl-*D*-glucamine (196 mg; 1 mmol) and sodium carbonate (212 mg; 2 mmol). The resulting mixture was stirred at room temperature for 5 minutes, and the solvent was evaporated under reduced pressure at room temperature. The resulting solid residue was mixed with dichloromethane (50 ml) and water (20 ml). The dichloromethane layer was separated, washed with 10% sodium carbonate (3×10 ml) and water (3×10 ml), and dried over anhydrous sodium carbonate.

After the solvent was evaporated, the solid residue was washed with hexane (3×5 ml) and dried in a vacuum under reduced pressure to give 350 mg (71%) of pure product. Selected signals for ^{1}H-NMR ($CDCl_3$) δ 7.71 (2H, d, J = 8.8 Hz), 7.67 (2H, d, J = 8.8 Hz), 3.17 (3H, s), and 1.66 (6H, s) ppm.

Preparation of 2-[4-(4-Chlorobenzoyl)phenoxy]-2-methyl-1-[4-(morpholin-4-yl)piperidin-1-yl]propan-1-one (PP4). FA chloride prepared from FA (160 mg; 0.5 mmol) and oxalyl chloride (0.25 mL; 380.1 mg; 3 mmol) as described for preparation of PP1 was dissolved in dichloromethane (30 ml) and mixed with tetrahydrofuran (10 ml) solution of 4-morpholinopiperidine (100 mg; 0.6 mol), and water (10 ml) solution of sodium carbonate (106 mg; 1 mmol). The resulting mixture was stirred at room temperature for 1 hour. Water (20 ml) was added, and the organic layer was separated and extensively washed with 5% hydrochloric acid (5×20 ml), water (3×10 ml), 10% sodium carbonate (5×20 ml), and water again (3×10 ml). After drying over anhydrous sodium carbonate, the solvent was evaporated to give the pure oil product (200 mg; 85%) that crystallized by standing at room temperature overnight. [If necessary, the product can be further purified by crystallization from hexane or by silica gel chromatography with ethyl acetate–ethanol (5:1)]. ^{1}H-NMR ($CDCl_3$) δ 7.71 (2H, d, J = 7.6 Hz), 7.68 (2H, d, J = 7.6 Hz), 7.47 (2H, d, J = 7.6 Hz), 6.92 (2H, d, J = 7.6 Hz), 4.66 (1H, d, J = 13.2 Hz), 4.60 (1H, d, J = 13.2 Hz), 3.64 (4H, t, J = 4.8 Hz), 2.90 (1H, t, J = 12.8 Hz), 2.57 (1H, t, J = 13.2 Hz), 4.38 (4H, m), 2.28 (1H, t of t, J_1 = 11.2 Hz, J_2 = 4 Hz), 1.83 (1H, d, J = 13.2 Hz), 1.71 (6H, s), 1.64 (1H, d, J = 13.2 Hz), 1.30 (1H, m), and 0.95 (1H, m) ppm.

Detection of PP Compounds by High-Performance Liquid Chromatography (HPLC)

All HPLC data were obtained from the Agilent 1100 apparatus equipped with a line degasser, binary pump (high pressure mixer), autosampler, column thermostat, and Diode Array Detector (Agilent Technologies, Santa Clara, CA). The analytical column (3 μm, 4.6×150 mm; Octyl Silane C8; YMC America, Inc.), solvent A–50 mM acetic acid in water, and solvent B–acetonitrile with isocratic flow were used to detect and quantify PP compounds in culture media and in cells, tissues, and body fluids. The flow rate was set to 1 ml/min, column temperature was 20 °C, and the sample volume was 5 μl. Diode Array Detector wavelength was set to 285 nm.

Sample Preparation. Blood, cell culture media, and cellular and tissue lysates were deproteinized by adding 150 μl of acetonitrile to 150 μl of sample, mixed well, and centrifuged (15,000*g*, 5 minutes). The lysates were sonicated on ice and centrifuged (15,000*g*, 5 minutes). Finally, 150 μl of the supernatant was mixed with the equal volume of acetonitrile, filtered through 0.22-μm centrifuge filter (Sigma), and analyzed by HPLC.

Cell Culture

We have used two human glioblastoma cell lines, LN-229 (ATCC# CRL-2611) and U-87MG (ATCC# HTB14); GBM12, which are patient-derived human glioblastoma cells [13,14], and the mouse glioblastoma cell line GL261-Red-FLuc (Bioware Brite; PerkinElmer# BW134246). All cell lines were maintained as semiconfluent monolayer cultures in DMEM (1 g/l glucose; with sodium pyruvate and L-glutamine) supplemented with 100 U/ml penicillin, 100 μg/ml streptomycin, and 10% fetal bovine serum (FBS) at 37°C in a 5% CO_2 atmosphere. The cells were treated with PP compounds at different doses ranging from 5 to 50 μM. In addition, the cells were treated with FF (Sigma Aldrich, St. Louis, MO) at concentrations ranging from 10 to 50 μM. Control cultures were treated with the corresponding volumes of DMSO (vehicle control; final concentration 0.1%). GBM12 cells were routinely propagated in the subcutaneous tissue of nude mice and isolated from the tumor tissue for short-term cultures as previously described [11] and according to IACUC protocol #3444 5 (LSUHSC, New Orleans, LA).

Evaluation of Metabolic Parameters

Metabolic responses of human glioblastoma cells were evaluated with Extracellular Flux Analyzer XFe24 (Agilent Technologies). During the day prior to each assay, the cells were plated at 4×10^4 cells/well in Agilent Seahorse 24-well XF cell culture microplates with growth-supporting media and incubated overnight. At the time of measurement, growth media were replaced with serum-free XF assay medium (Seahorse XF Base Medium supplemented with 1 mM sodium pyruvate, 2 mM glutamine, and 5.5 mM glucose), and cartridges equipped with oxygen-sensitive and pH-sensitive fluorescent probes (Seahorse) were placed above the cells. The oxygen consumption rate (OCR; indicative of mitochondrial respiration) and extracellular acidification rate (ECAR; indicative of glycolysis) were evaluated after injecting the PP compounds (all used at 25 μM), FF (50 μM), or DMSO (0.1%; vehicle control) followed by injections of metabolic toxins, including oligomycin (inhibitor of ATP synthase; 0.5 μM), carbonylcyanide-p-trifluoromethoxyphenylhydrazone (FCCP; uncoupling factor; 0.5 μM), rotenone (inhibitor of mitochondrial complex I; 0.3 μM), and antimycin A (inhibitor of mitochondrial complex III; 0.3 μM).

PPAR Luciferase Assay

The PPAR transcriptional activity was determined by utilizing the JsTkpGL3 reporter plasmid, which contains a firefly luciferase gene driven by the PPAR responsive element (PPRE), which consists of three copies of the J site from the apo-AII gene promoter. Together with JsTkpGL3 plasmid HepG2 cells were transfected with pSV40-GLuc (New England Biolabs., Ipswich, MA) control plasmid expressing Gaussia luciferase under the control of the constitutive SV40 early promoter, used to normalize for efficiency of transfection. Twenty-four hours after transfection, the cells were incubated with ciglitazone (30 μM), FF, PP1, PP2, PP3, and PP4 (all 25 μM) for an additional 24 hours. The luciferase activity was detected with the Dual-Luciferase reporter assay system (Promega, Madison, WI), and the resulting luminescence was measured with Synergy 2 microplate reader (BioTek, Winooski, VT).

Cell Death Assays

Cell death was evaluated by assays based on cell membrane integrity. We used either the trypan blue exclusion test [15] or the GUAVA easyCyte 8HT flow cytometer with ViaCount reagent (Millipore) and Guava/ViaCount software for data analysis. Briefly, the cells were plated at 1×10^4 cells/cm^2 in 24-well plates in growth medium. After 24 hours, the medium was replaced by fresh growth medium containing PP compounds, FF, or 0.1% DMSO (vehicle control) and further incubated for the amount of time specified for each experiment. The cells were then harvested with 0.05% trypsin/EDTA, centrifuged, resuspended in PBS, and counted in a hemocytometer with trypan blue (0.4%, 1:1) or incubated with the ViaCount reagent (1:10; 5 minutes at room temperature) before cell

viability was assessed by the Guava/ViaCount according to the manufacturer's recommendations.

Animal Studies

All described procedures involving experimental animals were performed in accordance with the IACUC protocol #3444 at LSUHSC, New Orleans.

Intracranial Tumor Growth. C57BL/6NHsd mice, 11-12 weeks of age (Envigo), were anesthetized with 4% isoflurane and secured in a stereotaxic head frame (Harvard Apparatus, Holliston, MA). GL-261-Red-Fluc cells (1×10^5 cells suspended in 2 μl of PBS) were injected into the brain parenchyma (coordinates: 3 mm anterior to bregma; 1.5 mm lateral to sagittal suture; 3 mm down from surface) through a burr hole in the skull using a 10-μl Hamilton syringe. Biophotonic images of the skull were captured using a Xenogen IVIS 200 imaging system (Palo Alto, CA) 2 weeks after initial cell implantation (Figure 6*C*). Prior to imaging, each mouse received an intraperitoneal injection of 100 μl of D-luciferin (30 mg/ml solution; PerkinElmer, Waltham, MA) and was anesthetized by isoflurane inhalation. The resulting images were evaluated, and luminescence measurements from equivalent regions of interest encompassing the entire skull were collected using Living Image 4.1 software (Xenogen).

Treatment. C57BL mice bearing well established intracranial mouse glioblastoma tumors (GL-261) were treated with PP1 (50 mg/kg/day, dissolved in 2% DMSO) administered by oral gavage. Control mice were treated with equal volume of the solvent. Following 14 days of daily drug or solvent administration, the animals were euthanized according to the standard ethically accepted procedure, and the following organs/body fluids were collected: blood, liver, kidneys, spleen, heart, intact brain, and intracranial tumors. These tissues were subjected to sample preparation for the HPLC analysis (PP1 tissue content) and for the routine pathological evaluation.

Pathological Evaluations. After harvesting the brain and tumors, liver, spleen, kidneys, heart, and lungs, the tissues were placed in 10% buffered formalin for 24 hours, processed, and embedded into paraffin blocks. Sections were cut at 4 μm in thickness, placed in electromagnetically charged slides, deparaffinized, rehydrated, and stained with hematoxylin and eosin for routine histopathological examination.

Statistical Analysis

Data were analyzed by a Student's *t* test corrected for multiple comparisons using Bonferroni-Dunn method. The differences between control and experimental groups were considered significant and marked with an asterisk (*) for *P* values lower or equal .05.

Results

Synthesis of New FF-Based Compounds for Glioblastoma Therapy

We have modified certain specific physiochemical properties of FF to improve its resistance to blood and tissue esterases, water solubility, tissue uptake, and ultimately anticancer activity. As a result, we have generated 26 new compounds, which have been designated here as PP compounds. They all contain a structural motif outlined in Figure 1*A*. Specifically, we have replaced the ester group that is present in FF with different amide groups. This is because amide hydrolysis rate under physiological conditions is substantially slower than esters [16,17]. In contrast, esters such as FF are readily cleaved by hydrolytic reactions catalyzed by acids, bases, metal ions, and hydrolytic proteins such as human serum albumin [18], and more specifically by blood and tissue esterases [4,19–22]. Unless designed with specific functional groups, amide bonds are rarely cleaved by chemical hydrolysis under physiological conditions, and their chemical cleavage requires harsh conditions such as high temperature in combination with the presence of strong acids or bases [16]. In addition to higher resistance to the hydrolyses, tertiary amides have higher water solubility as compared to esters and to primary or secondary amides. Based on our computational and biological studies, we had initially selected four compounds (PP1-PP4) for further analyses (Figure 1*A*). Preparation procedures for these compounds are outlined in Figure 1*B* and described in the Methods section. There are two feasible methods that are commonly used in organic synthesis for preparation of amides from carboxylic acid: a) through acid chlorides and b) by activating carboxylic acid with carbodiimides [23]. FA was used as a primary substrate and was converted into the corresponding acid chloride with oxalyl chloride. This chloride was coupled with secondary amine in basic media resulting in preparation of the PP compounds. Isolated yields were good to excellent, and the products (PP1-PP4) were purified by extraction and crystallization.

Computed physicochemical properties of the four preselected PP compounds are presented in Table 1. Using computational methods for the estimation of physicochemical properties of potential new lead compounds is well established in medicinal chemistry [24,25]. If we compare our computed descriptors to one obtained from lead compounds with anticancer activity [25], our amides PP1, PP2, and PP4 are well in the desired range (Table 1). Molecular weight should be around 380, ClogP around 3.7, PSA around 80, and HBA around 5. On the other hand, PP3 was designed to substantially increase water solubility, and it is a saccharide derivative that was perfectly reflected on its estimated physicochemical properties. It is well hydrated (5 hydrogen bond donors and 16 hydrogen bond acceptors) in water media, and it is hydrophilic (low ClogP); however, it has a large polar surface area that might decrease its cell membrane permeability [26].

In Vitro Anticancer Effects of PP Compounds Compared to FF

Since FA was used as a primary substrate for the proposed chemical modifications (Figure 1) and FA has only marginal anticancer properties in comparison to unprocessed FF [11], we have first tested to see if the new compounds (PP1-PP4) are indeed cytotoxic. We used two human glioblastoma cell lines (LN-229 and U87MG), patient-derived glioblastoma cells (GBM12), and a mouse glioblastoma cell line (GL-261) in this evaluation. Results in Figure 2*A* demonstrate changes in the percentage of cell death in LN-229 cells cultured in 10% FBS ± PP1, PP2, PP3, and PP4. All compounds were used at 5, 10, 25, and 50 μM, and the cells were treated for 24, 48, 72, and 96 hours. The control cultures were treated either with an equal volume of the vehicle (DMSO), or with 25 and 50 μM FF (positive control). In DMSO-treated cultures, the average cell death varied from 6%±1.4% to 7%±1.2% (Figure 2, *A* and *B*). In the presence of 50 μM FF (single dose), LN-229 cells demonstrated 24% ±4% cell death at 48 hours; 90%±1% at 72 hours, and 99%±1.2% at 96 hours. In contrast, 25 μM FF was not cytotoxic; however, the treated cells demonstrated a significant growth arrest (Figure 2*B*). Next, we compared FF data to PP1, PP2, PP3, and PP4. Similar to FF, all four compounds showed no cytotoxic effects during the first 48 hours following the treatment at all concentrations (Figure 2*A*). At

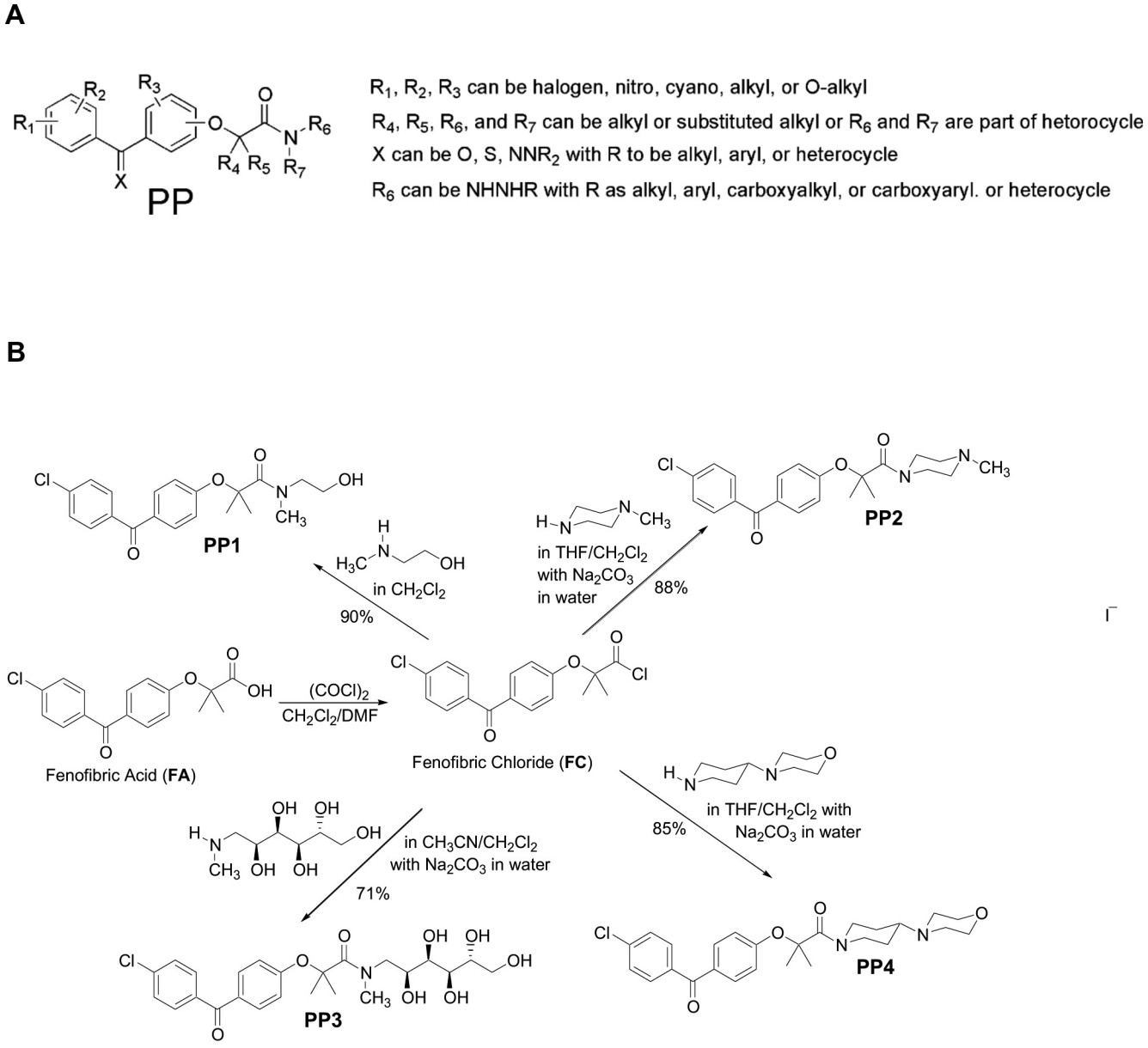

Figure 1. (A) General structural motif of PP compounds. All starting materials were reagent grade purchased from Sigma-Aldrich or Ark Pharm. ^{1}H-NMR spectra were recorded on Varian Mercury Plus 400-MHz instrument in $CDCl_3$ or DMSO-d_6, with the solvent chemical shifts as an internal standard. All computed molecular descriptors were generated by Chemaxon MarvinSketch version 18.8.0. (B) Strategies for the preparation of PP compounds (see Methods for details).

72- and 96-hour time points, PP1, PP2, and PP4 triggered extensive cell death at both 25 and 50 μM. This strong cytotoxicity was also observed at 10 μM PP1 (92%±2% cell death) and at 5 μM PP1 (74%±3% cell death); all four compounds were cytostatic at 5 μM (Figure 2, *C-F*), and FF was cytostatic at 25 μM (Figure 2*B*). In contrast to PP1, PP2, and PP4, PP3 demonstrated kinetics of growth retardation and cytotoxicity similar to FF (Figure 2, *A* and *B*). Like FF, PP3 was cytotoxic only at 50 μM and demonstrated cytostatic activity at 10 μM (Figure 2, *A* and *B*). We also observed extensive accumulation of peroxisomes in cells treated with PP3, which resembled morphology of LN-229 cells treated with 50 μM FF (not shown). This is also consistent with the data showing that PP3 does not repress PPREs (Figure 4*C*). Therefore, the anticancer activity of PP3 could be different from PP1, PP2, and PP4 and more similar to FF. However, PP3 dissolved in DMSO was unstable and needed to be prepared fresh for each experiment (data not shown).

On the basis of these initial findings, we have selected PP1 for additional experiments and confirmed its high *in vitro* cytotoxicity in

Table 1. Computed Properties for FF, FA, and Selected PP Compounds (PP1-PP4)

Comp.	MW	CLogP	HBD	HBA	MP	PSA	MSA	LogS
FF	360.83	5.28	0	6	38.18	52.60	533.56	−5.86
FA	318.75	4.36	0	9	32.42	63.60	437.06	−1.32
PP1	375.85	3.31	1	8	39.25	66.84	551.21	−5.09
PP2	400.90	3.85	0.33	6.67	43.10	49.85	597.80	−4.95
PP3	495.95	0.79	5	16	49.10	147.76	700.92	−4.48
PP4	470.99	3.81	0.73	8.27	50.43	59.08	707.09	−5.15

PP compounds = chemically modified FA; CLogP = calculated partitioning; HBD = hydrogen bond donor at pH = 7; HBA = hydrogen bond acceptor at pH = 7; MP = molecular polarizability (Å^3); polar surface area (Å^2); molecular surface area (Å^2); LogS = solubility (mg/ml) at pH = 7.

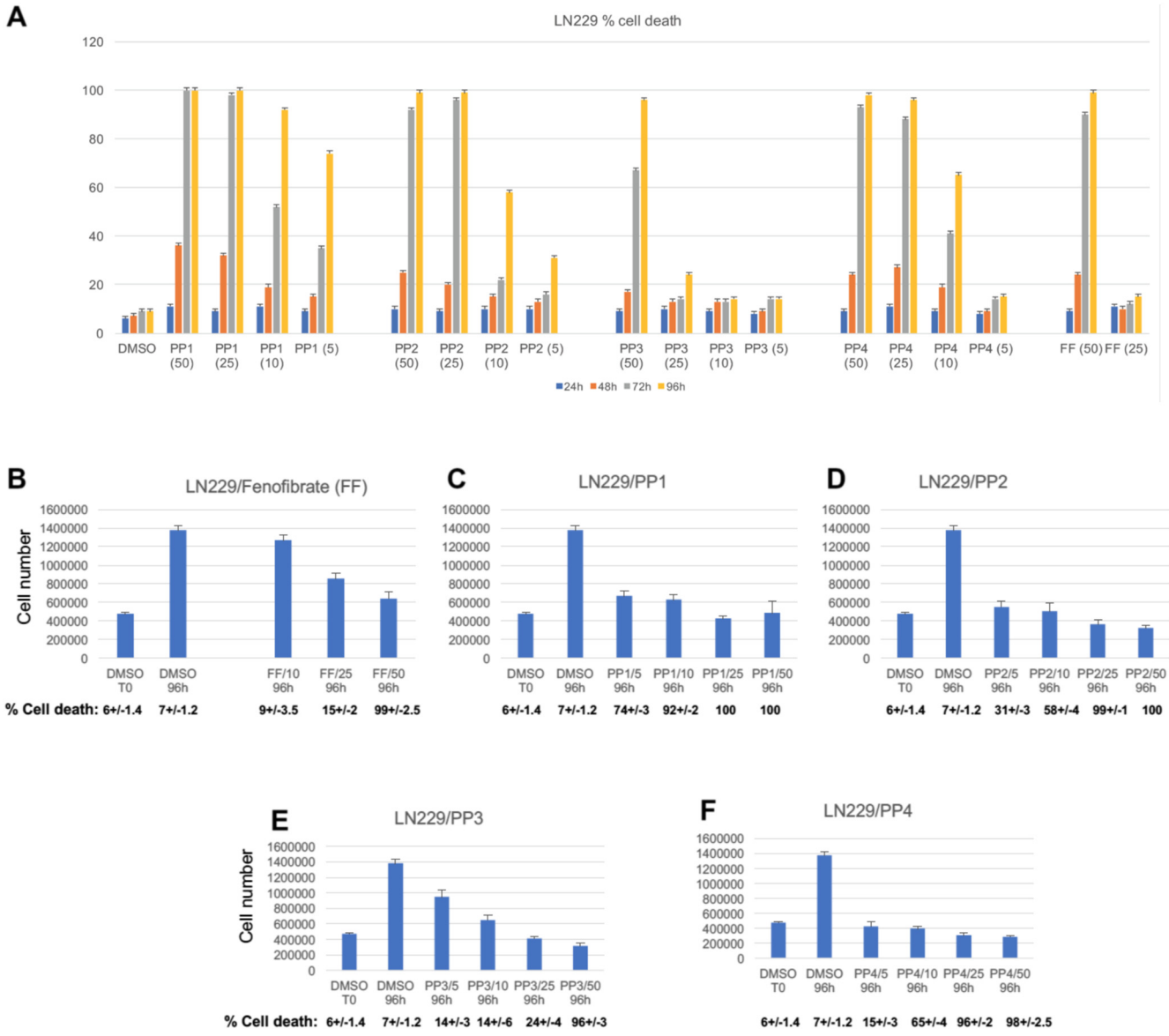

Figure 2. Cytotoxic (A) and cytostatic (B) effects of PP compounds. (A) Human glioblastoma cells, LN-229 (ATCC CRL-2611), were cultured in six-well plates at 2×10^5 /well in DMEM containing 10% FBS. The percentage of cell death (A-F) and the total cell number (B-F) were calculated at time 0 (T0; 6 hours after plating; plating efficiency) and at 24, 48, 72, and 96 hours after treatments. The cells were treated with FF at 10, 25, and 50 μM (FF/10, FF/25, and FF/50) and with PP1, PP2, PP3, and PP4 at 5, 10, 25, and 50 μM. Control cultures were treated with corresponding volumes of DMSO, which was used as a solvent for both FF and PP compounds. At the end point of each experiment, the cells were harvested in a quantitative manner, treated with 0.4% trypan blue solution (Sigma), and counted using bright field hemocytometer. Data represent average values from three independent experiments in triplicate ($n = 9$) ± SD. * indicates PP1 or PP2 or PP3 or PP4 values significantly different from the corresponding time point values for DMSO treatment. In B-F, both trypan blue–positive and trypan blue–negative cells were included in the calculation of cell number, and % cell death is indicated at the bottom of the corresponding column. Data represent average values ± SD ($n = 3$). * indicates PP1 or PP2 or PP3 or PP4 values significantly different from the DMSO value at 96 hours.

another human glioblastoma cell line, U87MG (Figure 3*A*); in patient-derived glioblastoma cells (GBM12) [13,27] (Figure 3*B*); and in the mouse glioblastoma cell line GL261 (Figure 3*C*).

Physiochemical and Metabolic Effects of PP Compounds Compared to FF

The main purpose for the described chemical modifications was to generate new compounds, which in comparison to FF are more stable, more resistant to blood and tissue esterases, better soluble in water, and possibly more effective in penetrating BBTB. Our data show that, in comparison to FF, PP1 was significantly more resistant to blood esterases (Figure 4*A*). In this experiment, 50 μM of PP1 and 50 μM of FF were incubated with human blood at 37°C at indicated time points. Following 48-hour incubation, almost all FF was converted to FA (Figure 4*A*; *right panel*). In contrast, nearly 25 μM of PP1 was still detected at the 48-hour time point (Figure 4*A*; *left panel*). In addition, we also demonstrate that, in comparison to FF, PP1 is much more soluble in water (Figure 4*B*), further supporting its potential as a new anticancer drug.

We have also demonstrated that PP1, PP2, and PP4 attenuated PPREs (Figure 4*C*). This unexpected finding indicates that these

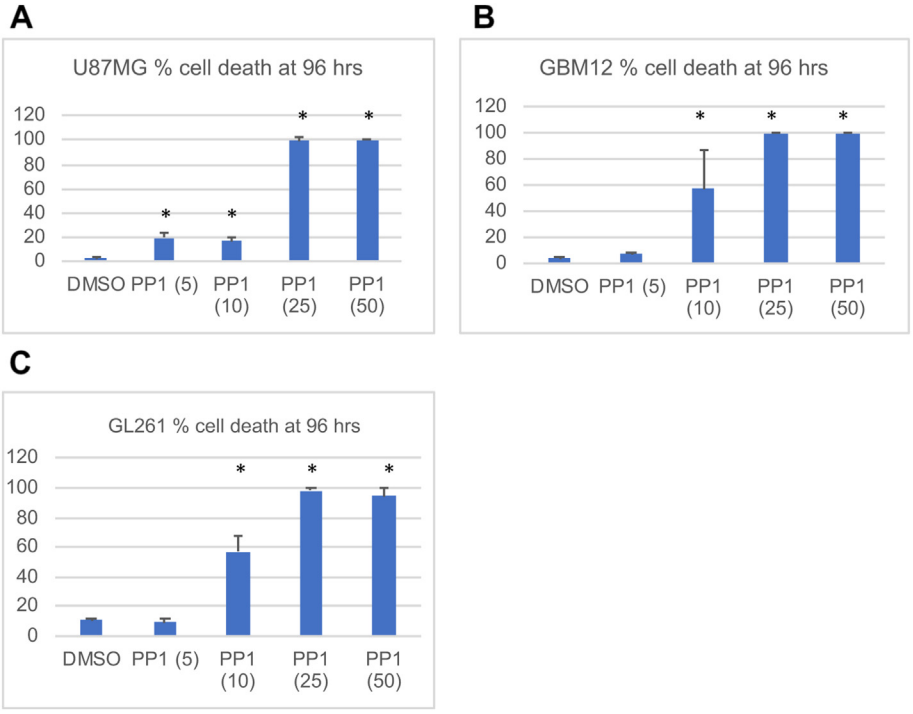

Figure 3. Cytotoxic effects of PP compounds evaluated in three different glioblastoma cell lines. (A) Human glioblastoma cell line U-87MG (ATCC# HTB14); (B) GBM12 cells, which are patient-derived human glioblastoma cells [54]; (C) and mouse glioblastoma cell line GL-261-luc (PerkinElmer Inc.) (C) were all cultured in 24-well plates at the initial density of 1×104 cells/cm^2 in DMEM containing 10% FBS. The percentage of cell death was calculated at 96-hour time point for all experimental conditions. The cells were treated with PP1 at 5, 10, 25, and 50 μM, and control cultures were treated with corresponding volumes of DMSO (PP1 solvent). At the end of each experiment, the cells were harvested in a quantitative manner, treated with 0.4% trypan blue solution (Sigma), and counted using bright field hemocytometer. Data represent average values ± SD from three independent experiments in triplicate ($n = 9$). * indicates PP1 values significantly different from DMSO.

three new compounds may have a different effect on tumor cells in comparison to FF, which following its conversion to FA becomes a potent agonist of PPARα. In contrast, PP3 does not share this PPAR-inhibitory activity, and its action on glioblastoma tumor cells could be more similar to FF (see also Figure 2, *A* and *B*).

Since FF anticancer effects are mediated mainly by the inhibition of mitochondrial respiration [11], we used an Extracellular Flux Analyzer (XF24, Seahorse Biosciences) to measure real-time OCR (indicative of mitochondrial respiration) and ECAR (indicative of glycolytic activity) in LN229 human glioblastoma cells treated with the PP1 at 25 μM concentration. The cells treated with DMSO (vehicle) or with 25 μM FF were used as a background control and positive control, respectively. These metabolic parameters were measured in monolayer cultures after sequential injections of the following metabolic toxins: oligomycin [inhibitor of complex V (ATP synthase)], FCCP (mitochondrial uncoupling factor); rotenone [inhibitor of mitochondrial complex I (NADH dehydrogenase)], and antimycin A (inhibitor of mitochondrial complex III). In a typical "mitochondrial stress" experiment (Figure 5), addition of FF and PP1 resulted in a dramatic decrease of OCR values and the corresponding increases in ECAR. Similar results were obtained for PP2, PP3, and PP4 (not shown). OCR and ECAR values in the control (DMSO) were practically unaffected (blue plot). In DMSO-treated controls, addition of oligomycin inhibited OCR, addition of FCCP resulted in a maximal increase of OCR values, and finally addition of rotenone completely blocked the oxygen consumption, as expected (Figure 5, *A* and *B*). Conversely, cells treated with either FF or PP1 demonstrated repressed oxygen consumption, accompanied by increased ECAR values (glycolysis) throughout the experiment. Other relevant metabolic parameters calculated from this experiment confirmed extremely low ATP production and almost none existing spare respiratory capacity in the cells treated with either with FF or with PP compounds (Figure 5*A*).

PP1 Tissue Distribution and Toxicity Evaluated in Large Intracranial Glioblastomas

We used a syngeneic mouse glioblastoma model in which GL-261-luc cells (PerkinElmer Inc.) were injected into the brain parenchyma of C57BL/6 mice. Following 2 weeks of a continuous tumor growth, mice with well-established, large intracranial tumors were selected using biophotonic imaging (Xenogen IVIS 200) (Figure 6*C*). We have selected mice with large tumors mostly because, in glioblastoma patients, the tumors are detected late usually and often are too big or located in brain areas, which prevent successful surgical resection. Control mice were treated with DMSO (vehicle), and experimental mice were treated with the PP1 at 25-75 mg/kg/day, administered by oral gavage. Following 14 days of drug administration, mice were euthanized and the following organs were collected: blood, liver, kidneys, spleen, heart, intact brain, and intracranial tumors. Both tumor-free and tumor-bearing mice were used for HPLC-based measurement of PP1 tissue distribution (Figure 6*A*) and for tissue toxicity analyses (Figure 6, *B*, *D* and *E*). Results in Figure 6*A* demonstrate that PP1 accumulates in all tissues examined, and importantly, an average concentration of the compound found in

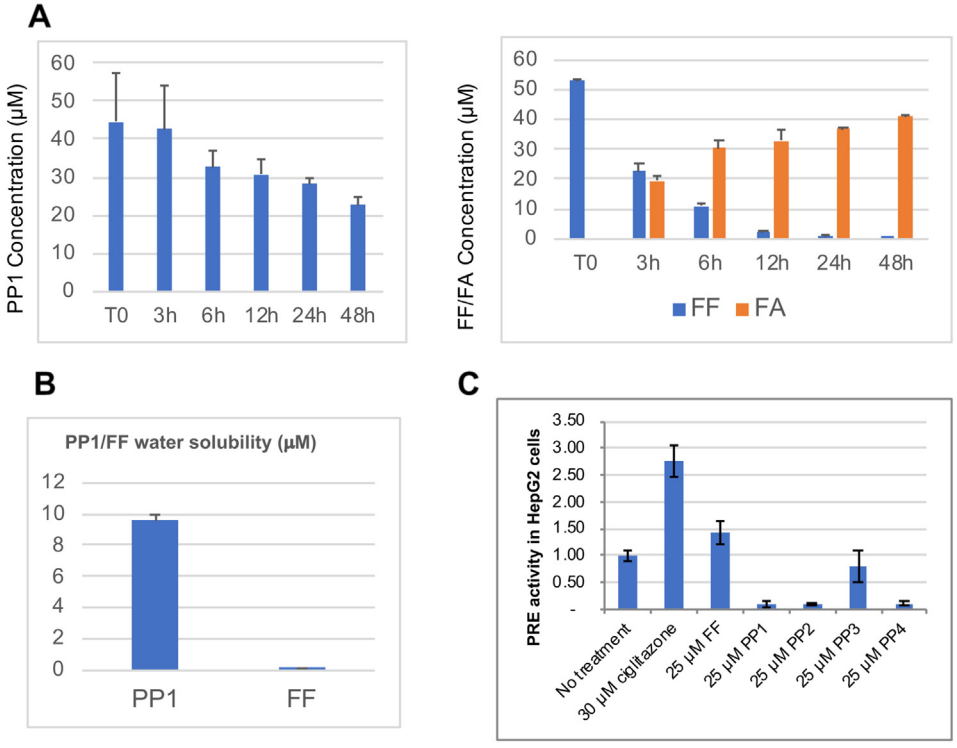

Figure 4. (A) Stability of PP1 and FF in human blood. Aliquots of 50 μM PP1 and FF in DMSO were added to 500 μl to heparinized human blood to a final concentration of 50 μM. Following incubation at 37°C for the indicated time points, the samples were frozen at −80°C and later prepared for HPLC-based detection of the compounds. Please note that FF is converted to FA in the presence of human blood. In the same condition, PP1 remains stable for a significantly longer time, and FA is not produced. Data represent average values with standard deviation ($n = 3$). (B) Water solubility. FF and PP1 were added to water to a final concentration of 50 mM and sonicated in an ultrasonic bath (Branson 1510 Digital Heated Ultrasonic bath) for 1 hour at room temperature. The samples were then centrifuged for 10 minutes at 16,000*g*, and the supernatant was filtered through 0.45-μm syringe filter. Water-solubilized PP1 and FF were subsequently processed for HPLC analysis (see Methods). Data represent average values with standard deviation ($n = 3$). (C) Effects of PP compounds on PPREs. The PPAR transcriptional activity was determined in HepG2 cells by the JsTkpGL3 reporter plasmid, which contains a firefly luciferase gene driven by the PPRE, which consists of three copies of the J site from the apo-AII gene promoter. To normalize for efficiency of transfection, the cells were additionally transfected with the pSV40-GLuc (New England Biolabs, Ipswich, MA) control plasmid. Twenty-four hours after transfection, the cells were incubated with ciglitazone (30 μM), FF, PP1, PP2, PP3, and PP4 (all 25 μM) for an additional 24 hours. The luciferase activity was detected with Dual-Luciferase reporter assay system (Promega, Madison, WI), and the resulting luminescence was measured with Synergy 2 microplate reader (BioTek, Winooski, VT). Data represent average values with standard deviation ($n = 6$).

intracranial tumors was 5.8 ± 0.7 μM. According to our *in vitro* data (Figure 2), this concentration could be therapeutically relevant. The highest PP1 accumulation was found in the liver (10.3 ±4.3 μM) and in the kidney (8.8 ± 4.7). In the blood, spleen, heart, and intact brains, the levels were 3.05 ± 0.2, 7.6 ± 3.2, 6.1 ± 2.4, and 4.9 ± 3.4 μM, respectively. Importantly, both tumor-free and tumor-bearing mice treated with PP1 did not show any major signs of toxicity to PP1 and maintained their body weight during the course of the treatment (Figure 6*B*). However, histological evaluation of the PP1-treated mice demonstrated inflammation and focal necrotic areas in the liver and an enlarged spleen with accumulation of hemosiderin (Figure 6*D*). In contrast, heart, kidney, and brain tissue showed no signs of pathology (Figure 6*D*).

Results in Figure 6*C* demonstrate four examples of intracranial tumors selected for the treatment. In this experiment, the tumors were allowed to grow for 14 days before treatment. Subsequently, mice with large intracranial tumors were selected using the biophotonic imaging and treated either with DMSO (vehicle) or with PP1 (50 mg/kg/day; oral administration). Although our data do not show obvious signs of the tumor regression following the treatment, most likely because tumors were already too big for a successful intervention, we detected large areas of tumor cell death found exclusively in mice treated with PP1, indicating a positive effect of the treatment (Figure 6*E*). In contrast, DMSO-treated mice had only small and sparse areas of necrosis (Figure 6*E*). In this experiment, both control and PP1-treated mice were euthanized at the same time when mice started to demonstrate signs of distress. Importantly, large necrotic areas found exclusively in PP1-treated animals indicate a promising therapeutic potential of this new metabolic drug.

Discussion

Glial tumors account for nearly 50% of all adult primary intracranial neoplasms, among which glioblastoma is the most aggressive and practically incurable [28,29]. A large variety of different genetic and epigenetic modifications have been found in glioblastomas, among which p53 mutations, EGF receptor amplification, and PTEN mutations are most common [30]. However, gene therapy, molecular and immunological approaches targeting these molecules and their pathways, as well as recently tested antibodies against immune

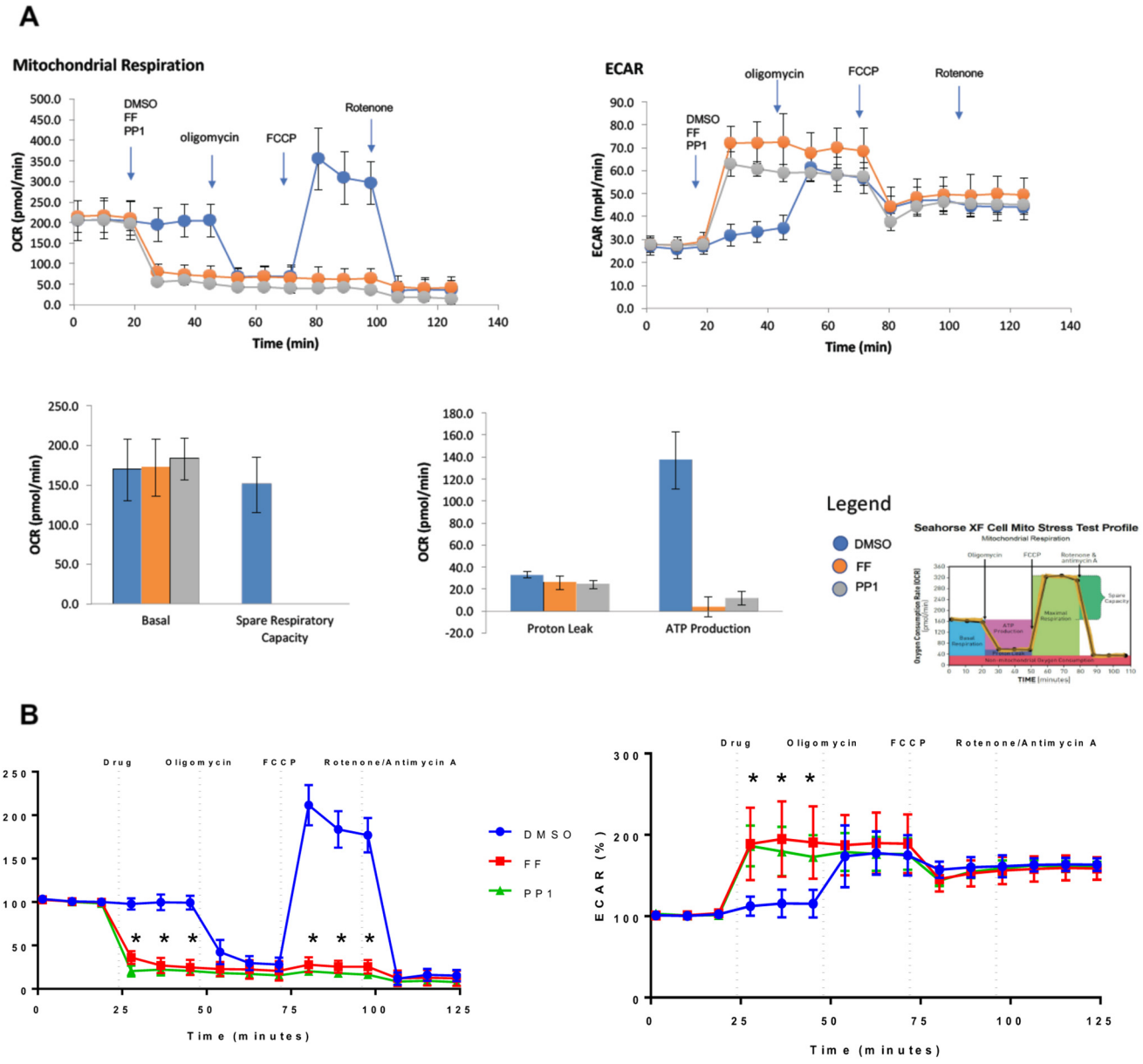

Figure 5. Metabolic effects of PP compounds compared to FF. Metabolic responses of LN-229 human glioblastoma cells were evaluated with Extracellular Flux Analyzer XF24 (Seahorse Biosciences, North Billerica, MA). Prior each assay, the cells were plated at 4×10^4 cells/well in 24-well plates in growth supporting media. At the time of measurement, growth media were replaced with serum-free XF medium (Seahorse) in cartridges equipped with oxygen-sensitive and pH-sensitive fluorescent probes. The OCR (indicative of mitochondrial respiration) and ECAR (indicative of glycolysis) were evaluated after injecting the following metabolic toxins: oligomycin, FCCP, rotenone, and antimycin A. Immediate metabolic effects were determined by comparing OCR and ECAR values in cells preincubated with DMSO (vehicle) or with PP1 and FF; all used at 25 μM. (A) Representative experiment in which real OCR (pmol/min) and ECAR (mpH/min) values are shown. Other relevant metabolic parameters calculated from this experiment include ATP production, spare respiratory capacity, basal OCR levels, and proton leak. (B) Average OCR and ECAR data (% change over basal OCR and ECAR values) from three independent experiments repeated five times ($n = 15$). Data represent average values ± SD. * indicates PP1 values significantly different from DMSO.

checkpoint inhibitors [31] have yet to produce improvements in patient outcomes. In addition to the introduction of the personalized medicine approach to target these specific pathways in glioblastoma patients [32–34], metabolic methods including calorie restriction and ketogenic diet are surprisingly effective as supplemental therapies for glioblastoma patients [35–37]. In addition, interesting anticancer effects of lipid-lowering drugs, fibrates, and statins have also been reported [3,8,38–42]. A 10-year all-cause mortality study involving 7722 patients treated with different fibrates revealed that the use of these metabolic compounds was associated with a significantly lower total mortality and reduced probability of death from cancer [43]. In cell culture and in animal studies, various members of the fibrate family demonstrated a broad range of anticancer activities [1–3,10,41,42,44–47]. These multiple reports encouraged clinical trials in which chronic administration of low doses of FF was tested along with chemotherapeutic agents, minimizing their toxicity and acute side effects in patients with recurrent brain tumors and leukemia [48,49]. Although these beneficial anticancer effects of FF

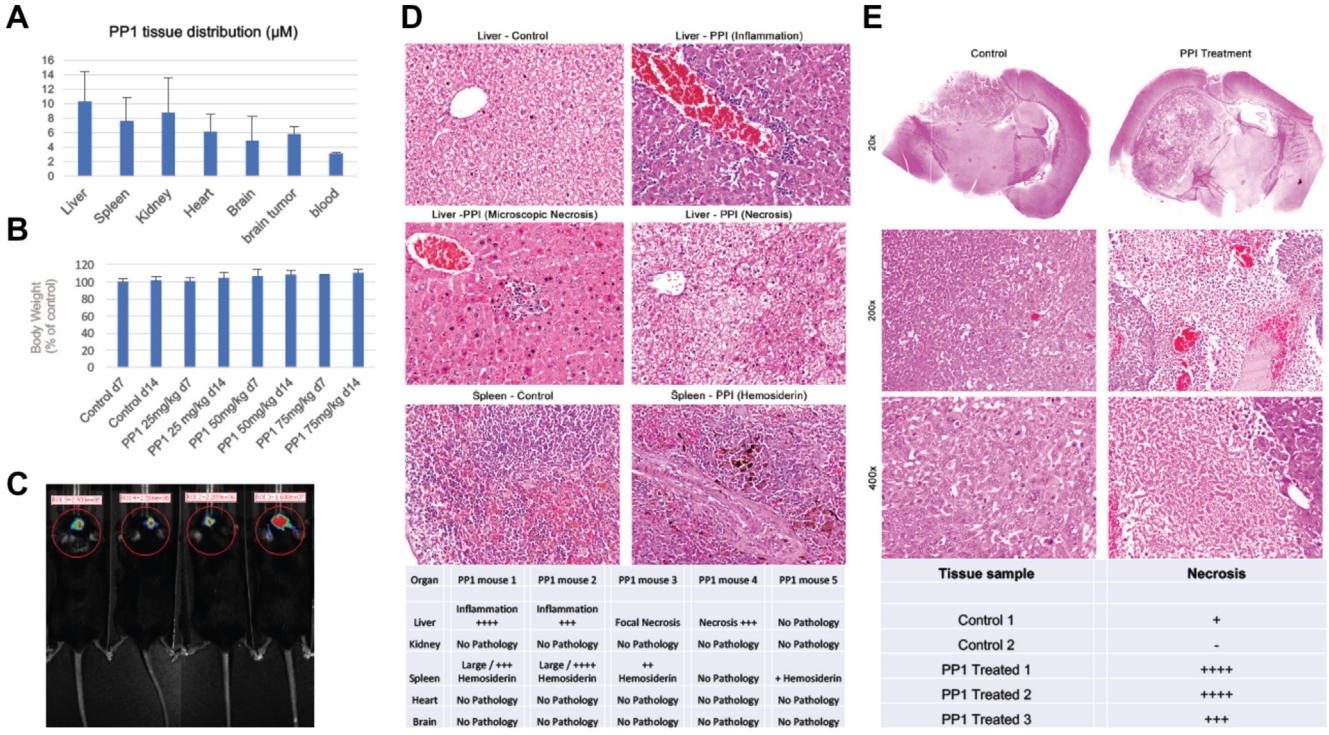

Organ	PP1 mouse 1	PP1 mouse 2	PP1 mouse 3	PP1 mouse 4	PP1 mouse 5
Liver	Inflammation ++++	Inflammation +++	Focal Necrosis	Necrosis +++	No Pathology
Kidney	No Pathology	No Pathology	No Pathology	No Pathology	No Pathology
Spleen	Large / +++ Hemosiderin	Large / ++++ Hemosiderin	++ Hemosiderin	No Pathology	+ Hemosiderin
Heart	No Pathology	No Pathology	No Pathology	No Pathology	No Pathology
Brain	No Pathology	No Pathology	No Pathology	No Pathology	No Pathology

Tissue sample	Necrosis
Control 1	+
Control 2	-
PP1 Treated 1	++++
PP1 Treated 2	++++
PP1 Treated 3	+++

Figure 6. PP1 tissue distribution and toxicity data. (A) PP1 accumulation in different tissues following oral administration of PP1 (25 mg/kg). C57BL/6 mice were treated daily for 14 days, and the levels of PP1 in the blood, liver, spleen, kidney, heart, brain, and brain tumors were evaluated by HPLC as previously described. Data represent average values with standard deviation ($n = 3$). (B) Body weight of C57BL/6 mice treated with PP1. Mice were treated with the PP1 at doses ranging from 25 to 75 mg/kg/day administered by oral gavage. Following 7 and 14 days of daily drug administration, both control (DMSO-treated) and experimental (PP1-treated) mice were weighted. Data represent average values with standard deviation (at least three mice per group were included). (A and B) Tumor-free and tumor-bearing mice were included for the body weight measurement. (C, D, and E) Intracranial growth of GL-261-Luc cells. C57 black mice, 6-8 weeks of age, were anesthetized with 4% isoflurane and secured in a stereotaxic head frame (Harvard Apparatus, Holliston MA). GL-261-luc cells (1×10^5 cells in 2 μl; PerkinElmer Inc.) were injected into the brain parenchyma (coordinates: 3 mm anterior to bregma; 1.5 mm lateral to sagittal suture; 3 mm down from surface) through a burr hole in the skull using a 10-μl Hamilton syringe. (C) Mice with large intracranial tumors were selected using bioluminescence imaging with Xenogen IVIS 200 system. Tumor size is expressed as radiance (photons/s/cm^2/sr) and was quantified with the Living Image 4.1 software according to the manufacturer's recommendations (Xenogen). (D and E) Pathological evaluation of intracranial tumors and tissues. Following 14 days of drug administration (control: DMSO administered daily by oral gavage; PP1 50 mg/kg administered daily by oral gavage), the animals were euthanized, and the following organs were collected: liver, kidneys, spleen, heart, and intact brain and intracranial tumors. The tissues were formalin fixed and paraffin embedded, and the resulting thin section were stained with hematoxylin and eosin for a routine pathological evaluation.

are still suspected to rely on PPAR-dependent mechanism/s, we have recently demonstrated that brain tumor cells retain sensitivity to FF in the presence of PPARα antagonists or PPARα siRNA [1,11]. This strongly suggests that FF may have additional PPARα-independent activity. Other groups also demonstrated that FF could have PPAR-independent cellular effects including PPAR-independent activation of GDF15 [50], effects of FF on cell membrane fluidity [51], and the FF-induced inhibition of mitochondrial respiration in isolated cardiac and liver mitochondria [52,53]. Therefore, a growing line of evidence supports the interaction of unprocessed FF (ester) with biological membranes, which could be a reason for the observed strong anticancer activity of this lipid-lowering drug. We have demonstrated previously that unprocessed FF (ester) accumulates in mitochondrial membranes [11]. As a consequence, the affected glioblastoma cells underwent immediate impairment of mitochondrial respiration and compensatory attempt of increasing glycolysis, which initially supported cell survival. However, prolonged (48 hours) exposure to FF depleted intracellular ATP and activated the AMPK-mTOR autophagy axis in glioblastoma cells. Although autophagy gave the affected cells an additional 12-24 hours of survival, it was ultimately followed by a massive tumor cell death [11].

In spite of these promising results, FF does not cross the blood-brain barrier (BBB) [4] and is quickly converted to FA by blood and tissue esterases (Figure 4*A* and [4]). We have made several chemical modifications in FF structure to address these problems. From the initial 26 new compounds, four with the most promising anticancer properties were evaluated in this study (Figure 1 and Table 1). These chemical modifications were designed to improve the compounds' stability, water solubility, tissue penetration, and ultimately anticancer potential. One of the lead compounds, PP1, is highly effective in triggered extensive glioblastoma cell death *in vitro* (Figures 2 and 3) and, similar to FF, induces immediate repression of mitochondrial respiration (Figure 5). In difference to FF, PP1 is much more stable when exposed to human blood (Figure 4*A*) and is significantly better soluble in water (Figure 4*B*). For animal studies, we have selected mice with large tumors. This is because in patients glioblastomas are detected late usually and often are too big for surgery or are located in brain areas, which prevent safe surgical resection. Although PP1-

treated mice did not show obvious signs of tumor regression, most likely because the selected tumors were too big for a successful treatment, large areas of tumor cell death found exclusively in mice treated with PP1 are highly encouraging. This is very important since brain tumors are particularly difficult to treat due to distinct anatomical and physiological traits of neural tissue and vasculature, BBTB. Although BBTB is more permeable than BBB, it still represents the major obstacle preventing anticancer agents from reaching therapeutically relevant concentrations. The only FDA-approved chemotherapy drug against glioblastoma which can cross BBB is temozolomide; however glioblastoma cells quickly develop temozolomide resistance, and recurrent tumors are practically incurable [13].

Our new metabolic compound, PP1, can be detected both in intact brain and in the brain tumors at μM concentrations following its oral administration. This is a very promising feature for glioblastoma therapy; however, we still do not understand why PP1 triggers extensive tumor cell death within the tumor mass but not in tumor-free normal brain. Although we do not have a definitive answer at this point, our previous data show that 50 μM FF was significantly less toxic to normal human astrocytes (NHA) compared to glioblastomas [11]. This is in spite of the immediate mitochondrial responses to FF, which are similar in both glioblastoma cells and in NHA [11]. This apparent discrepancy indicates that the observed low sensitivity of NHA to FF may involve mechanisms, which are not directly linked to FF-induced or PP1-induced inhibition of mitochondrial respiration. Further experiments are required to address this significant issue and, more specifically, to explain the difference between normal brain cells and brain tumor cells in responding to this new class of metabolic drugs.

Conclusions

We have evaluated the antiglioblastoma effects of four new compounds, which are modifications of a common lipid-lowering drug, FF. These four chemical modifications were developed specifically to increase the compounds' resistance to blood and tissue esterases, water solubility, brain tissue penetration, and ultimately antiglioblastoma potential. One of the lead compounds, PP1, is highly effective in blocking mitochondrial respiration and in eliminating glioblastoma cells *in vitro.* In comparison to FF, PP1 is also more stable when exposed to human blood and is better soluble in water. Our data from large intracranial glioblastoma tumors show that PP1 accumulates in the brain tumor tissue following oral administration and causes extensive glioblastoma cell death. Importantly, PP1-treated mice did not show any major signs of distress. Our results encourage the use of this new class of metabolic compounds as a part of antiglioblastoma therapy in the future.

Acknowledgements

We are grateful to Susan Theodosious for her editorial efforts. This work was supported by LSUHSC, Dean of School of Medicine matching funds (K.R.); and P20-GM121288-01 (K.R.). In addition, F. P. is supported by P20-GM121288-01 pilot project, and 1U54 GM104940 Louisiana Clinical and Translational Science Center. M. R. and E. Z. were supported by Faculty of Biochemistry, Biophysics and Biotechnology of Jagiellonian University, a partner of the Leading National Research Center (KNOW) supported by the Ministry of Science and Higher Education. Pathological evaluation was performed in collaboration with the LSUHSC/LCRC Molecular Histopathology and Analytical Microscopy Core (supported by P30GM114732-04 and P20-GM121288-01). All HPLC data were prepared in collaboration with LSUHSC/LCRC Cellular Immunology Metabolism Core (supported by P30GM114732-04 and P20-GM121288-01). Statistical evaluations were prepared in collaboration with LSUHSC Biostatistics Bioinformatics Core (partially supported by P20-GM121288-01), and *in vivo* animal imaging was performed in LSU Health Morphology and Imaging Core.

References

[1] Drukala J, Urbanska K, Wilk A, Grabacka M, Wybieralska E, Del Valle L, Madeja Z, and Reiss K (2010). ROS accumulation and IGF-IR inhibition contribute to fenofibrate/PPARalpha -mediated inhibition of glioma cell motility in vitro. Mol Cancer. **9**, 159 [Epub 2010/06/24. doi: 1476-4598-9-159 [pii] 10.1186/1476-4598-9-159. PubMed PMID: 20569465; PMCID: 2912247].

[2] Grabacka M, Placha W, Plonka PM, Pajak S, Urbanska K, Laidler P, and Slominski A (2004). Inhibition of melanoma metastases by fenofibrate. *Arch Dermatol Res* **296**(2), 54–58 [PubMed PMID: 15278363].

[3] Grabacka M, Plonka PM, Urbanska K, and Reiss K (2006). Peroxisome proliferator-activated receptor alpha activation decreases metastatic potential of melanoma cells in vitro via down-regulation of Akt. *Clin Cancer Res* **12**(10), 3028–3036 [PubMed PMID: 16707598].

[4] Grabacka M, Waligorski P, Zapata A, Blake DA, Wyczechowska D, Wilk A, Rutkowska M, Vashistha H, Ayyala R, and Ponnusamy T, et al (2015). Fenofibrate subcellular distribution as a rationale for the intracranial delivery through biodegradable carrier. *J Physiol Pharmacol* **66**(2), 233–247 [PubMed PMID: 25903954].

[5] Grabacka MM, Wilk A, Antonczyk A, Banks P, Walczyk-Tytko E, Dean M, Pierzchalska M, and Reiss K (2016). Fenofibrate induces ketone body production in melanoma and glioblastoma cells. *Front Endocrinol* **7**(5). http://dx.doi.org/10.3389/fendo.2016.00005 [PubMed PMID: 26869992; PMCID: 4735548].

[6] Jeansonne D, DeLuca M, Marrero L, Lassak A, Pacifici M, Wyczechowska D, Wilk A, Reiss K, and Peruzzi F (2015). Anti-tumoral effects of miR-3189-3p in glioblastoma. *J Biol Chem* **290**(13), 8067–8080. http://dx.doi.org/10.1074/jbc.M114.633081 [PubMed PMID: 25645911; PMCID: 4375465].

[7] Koltai T (2015). Fenofibrate in cancer:mechanisms involved in anticancer activity. *F1000Research* **4**(55), 1–22. http://dx.doi.org/10.12688/f1000research.6153.1.

[8] Panigrahy D, Kaipainen A, Huang S, Butterfield CE, Barnes CM, Fannon M, Laforme AM, Chaponis DM, Folkman J, and Kieran MW (2008). PPARalpha agonist fenofibrate suppresses tumor growth through direct and indirect angiogenesis inhibition. *Proc Natl Acad Sci U S A* **105**(3), 985–990 [Epub 2008/01/18. doi: 0711281105 [pii] 10.1073/pnas.0711281105. PubMed PMID: 18199835; PMCID: 2242705].

[9] Scatena R, Bottoni P, and Giardina B (2008). Mitochondria, PPARs, and cancer: is receptor-independent action of PPAR agonists a key?*PPAR Res* **2008**, 256251 [PubMed PMID: 18645611].

[10] Urbanska K, Pannizzo P, Grabacka M, Croul S, Del Valle L, Khalili K, and Reiss K (2008). Activation of PPARalpha inhibits IGF-I–mediated growth and survival responses in medulloblastoma cell lines. *Int J Cancer* **123**(5), 1015–1024 [PubMed PMID: 18546270].

[11] Wilk A, Wyczechowska D, Zapata A, Dean M, Mullinax J, Marrero L, Parsons C, Peruzzi F, Culicchia F, and Ochoa A, et al (2014). Molecular Mechanisms of Fenofibrate-Induced Metabolic Catastrophe and Glioblastoma Cell Death. *Mol Cell Biol*. http://dx.doi.org/10.1128/MCB.00562-14 [PubMed PMID: 25332241].

[12] Kraja AT, Province MA, Straka RJ, Ordovas JM, Borecki IB, and Arnett DK (2010). *Fenofibrate and metabolic syndrome. Endocr Metab Immune Disord Drug Targets* **10**(2), 138–148 [Epub 2010/04/22. doi: EMID-DT-ABS-33 [pii]. PubMed PMID: 20406163].

[13] Cen L, Carlson BL, Pokorny JL, Mladek AC, Grogan PT, Schroeder MA, Decker PA, Anderson SK, Giannini C, and Wu W, et al (2013). *Efficacy of protracted temozolomide dosing is limited in MGMT unmethylated GBM xenograft models. Neuro Oncol* **15**(6), 735–746. http://dx.doi.org/10.1093/neuonc/not010 [PubMed PMID: 23479134; PMCID: 3661094].

[14] Kitange GJ, Carlson BL, Schroeder MA, Grogan PT, Lamont JD, Decker PA, Wu W, James CD, and Sarkaria JN (2009). *Induction of MGMT expression is*

associated with temozolomide resistance in glioblastoma xenografts. Neuro-Oncology **11**(3), 281–291. http://dx.doi.org/10.1215/15228517-2008-090 [PubMed PMID: 18952979; PMCID: 2718972].

[15] Strober W (2015). *Trypan blue exclusion test of cell viability. Curr Protoc Immunol* **111**. http://dx.doi.org/10.1002/0471142735.ima03bs111 [A3 B 1-3. Epub 2015/11/04 PubMed PMID: 26529666].

[16] Testra B and Mayer J (2003). *Hydrolysis in Drug and Prodrug Metabolism: Chemistry, Biochemistry, and Enzymology*. John Wiley and Sons; 2003

[17] Wang P and Choi S (2015). *Mechanism of drug release in nanotherapeutic delivery systems. Chem Rev* **115**, 3388–3432.

[18] Salvi A, Carrupt P, Mayer J, and Testra B (1997). *Esterase-like activity of human serum albumin toward prodrug esters of nicotinic acid. Drug Metab Dispos* **25**, 395–398.

[19] Bahar FG, Ohura K, Ogihara T, and Imai T (2012). *Species difference of esterase expression and hydrolase activity in plasma. J Pharm Sci* **101**(10), 3979–3988. http://dx.doi.org/10.1002/jps.23258 [PubMed PMID: 22833171].

[20] Najib J (2002). *Fenofibrate in the treatment of dyslipidemia: a review of the data as they relate to the new suprabioavailable tablet formulation. Clin Ther* **24**(12), 2022–2050 [PubMed PMID: 12581543].

[21] Redinbo MR and Potter PM (2005). *Mammalian carboxylesterases: from drug targets to protein therapeutics. Drug Discov Today* **10**(5), 313–325. http://dx.doi.org/10.1016/S1359-6446(05)03383-0 [PubMed PMID: 15749280].

[22] Weil A, Caldwell J, and Strolin-Benedetti M (1990). *The metabolism and disposition of 14C-fenofibrate in human volunteers. Drug Metab Dispos* **18**(1), 115–120 [Epub 1990/01/01. PubMed PMID: 1970770].

[23] Valeur E and Bradley M (2009). *Amide bond formation: beyond the myth of coupling reagents. Chem Soc Rev* **38**(2), 606–631. http://dx.doi.org/10.1039/b701677h [Epub 2009/01/27 PubMed PMID: 19169468].

[24] Brown N (2015). *Silico Medicinal Chemistry: Computational Methods to Support Drug Design*. London: Royal Society of Chemistry; 2015 .

[25] Singh D (2016). *Defining desirable natural product derived anticancer drug space: optimization of molecular physicochemical properties and ADMET attributes. ADMET & DMPK* **4**(2), 98–113.

[26] Pajouhesh H and Lutz G (2005). *Medicinal chemical properties of successful cantal nervous system drugs. NeuroRx* **2**(4), 541–553.

[27] Lassak A, Dean M, Wyczechowska D, Wilk A, Marrero L, Trillo-Tinoco J, Boulares AH, Sarkaria JN, Del Valle L, and Peruzzi F, et al (2018). *Molecular and structural traits of insulin receptor substrate 1/LC3 nuclear structures and their role in autophagy control and tumor cell survival. Mol Cell Biol* **38**(10). http://dx.doi.org/10.1128/MCB.00608-17 [Epub 2018/02/28 PubMed PMID: 29483302; PMCID: PMC5954195].

[28] Nakada M, Nakada S, Demuth T, Tran NL, Hoelzinger DB, and Berens ME (2007). *Molecular targets of glioma invasion. Cell Mol Life Sci* **64**(4), 458–478 [PubMed PMID: 17260089].

[29] Terzis AJ, Niclou SP, Rajcevic U, Danzeisen C, and Bjerkvig R (2006). *Cell therapies for glioblastoma. Expert Opin Biol Ther* **6**(8), 739–749 [PubMed PMID: 16856796].

[30] Ohgaki H and Kleihues P (2007). *Genetic pathways to primary and secondary glioblastoma. Am J Pathol* **170**(5), 1445–1453 [PubMed PMID: 17456751].

[31] Romani M, Pistillo MP, Carosio R, Morabito A, and Banelli B (2018). *Immune checkpoints and innovative therapies in glioblastoma. Front Oncol* **8**, 464. http://dx.doi.org/10.3389/fonc.2018.00464 [Epub 2018/11/09. PubMed PMID: 30406030; PMCID: PMC6206227].

[32] Brennan CW, Verhaak RG, McKenna A, Campos B, Noushmehr H, Salama SR, Zheng S, Chakravarty D, Sanborn JZ, and Berman SH, et al (2013). *The somatic genomic landscape of glioblastoma. Cell* **155**(2), 462–477. http://dx.doi.org/10.1016/j.cell.2013.09.034 [PubMed PMID: 24120142; PMCID: 3910500].

[33] Network TC (2013). *Corrigendum: Comprehensive genomic characterization defines human glioblastoma genes and core pathways. Nature* **494**(7438), 506. http://dx.doi.org/10.1038/nature11903 [PubMed PMID: 23389443].

[34] Shen R, Mo Q, Schultz N, Seshan VE, Olshen AB, Huse J, Ladanyi M, and Sander C (2012). *Integrative subtype discovery in glioblastoma using iCluster. PLoS One* **7**(4)e35236. http://dx.doi.org/10.1371/journal.pone.0035236 [PubMed PMID: 22539962; PMCID: 3335101].

[35] Champ CE, Palmer JD, Volek JS, Werner-Wasik M, Andrews DW, Evans JJ, Glass J, Kim L, and Shi W (2014). *Targeting metabolism with a ketogenic diet during the treatment of glioblastoma multiforme. J Neuro-Oncol* **117**(1), 125–131. http://dx.doi.org/10.1007/s11060-014-1362-0 [PubMed PMID: 24442482].

[36] Maroon J, Bost J, Amos A, and Zuccoli G (2013). *Restricted calorie ketogenic diet for the treatment of glioblastoma multiforme. J Child Neurol* **28**(8), 1002–1008. http://dx.doi.org/10.1177/0883073813488670 [PubMed PMID: 23670248].

[37] Seyfried TN, Kiebish MA, Marsh J, Shelton LM, Huysentruyt LC, and Mukherjee P (2011). *Metabolic management of brain cancer. Biochim Biophys Acta* **1807**(6), 577–594. http://dx.doi.org/10.1016/j.bbabio.2010.08.009 [PubMed PMID: 20804725].

[38] Clendening JW and Penn LZ (2012). *Targeting tumor cell metabolism with statins. Oncogene* **31**(48), 4967–4978. http://dx.doi.org/10.1038/onc.2012.6 [PubMed PMID: 22310279].

[39] Egerod FL, Nielsen HS, Iversen L, Thorup I, Storgaard T, and Oleksiewicz MB (2005). *Biomarkers for early effects of carcinogenic dual-acting PPAR agonists in rat urinary bladder urothelium in vivo. Biomarkers* **10**(4), 295–309 [PubMed PMID: 16240504].

[40] Goard CA, Mather RG, Vinepal B, Clendening JW, Martirosyan A, Boutros PC, Sharom FJ, and Penn LZ (2010). *Differential interactions between statins and P-glycoprotein: implications for exploiting statins as anticancer agents. Int J Cancer* **127**(12), 2936–2948. http://dx.doi.org/10.1002/ijc.25295 [PubMed PMID: 21351272].

[41] Grabacka M and Reiss K (2008). *Anticancer properties of PPARalpha-effects on cellular metabolism and inflammation. PPAR Res* **2008**, 930705 [PubMed PMID: 18509489].

[42] Saidi SA, Holland CM, Charnock-Jones DS, and Smith SK (2006). *In vitro and in vivo effects of the PPAR-alpha agonists fenofibrate and retinoic acid in endometrial cancer. Mol Cancer* **5**(13) [PubMed PMID: 16569247].

[43] Gardette V, Bongard V, Dallongeville J, Arveiler D, Bingham A, Ruidavets JB, Amouyel P, Haas B, Ducimetiere P, and Ferrieres J (2009). *Ten-year all-cause mortality in presumably healthy subjects on lipid-lowering drugs (from the Prospective Epidemiological Study of Myocardial Infarction [PRIME] prospective cohort). Am J Cardiol* **103**(3), 381–386 [Epub 2009/01/27. doi: S0002-9149(08)01709-8 [pii] 10.1016/j.amjcard.2008.09.092. PubMed PMID: 19166693].

[44] Grabacka M, Pierzchalska M, and Reiss K (2013). *Peroxisome proliferator activated receptor alpha ligands as anticancer drugs targeting mitochondrial metabolism. Curr Pharm Biotechnol* **14**(3), 342–356 [PubMed PMID: 21133850; PMCID: 3631438].

[45] Shigeto T, Yokoyama Y, Xin B, and Mizunuma H (2007). *Peroxisome proliferator-activated receptor alpha and gamma ligands inhibit the growth of human ovarian cancer. Oncol Rep* **18**(4), 833–840 [Epub 2007/09/06. PubMed PMID: 17786343].

[46] Wilk A, Urbanska K, Grabacka M, Mullinax J, Marcinkiewicz C, Impastato D, Estrada JJ, and Reiss K (2012). *Fenofibrate-induced nuclear translocation of FoxO3A triggers Bim-mediated apoptosis in glioblastoma cells in vitro. Cell Cycle* **11**(14), 2660–2671 [Epub 2012/06/27. doi: 21015 [pii] 10.4161/cc.21015. PubMed PMID: 22732497; PMCID: 3409008].

[47] Yokoyama Y, Xin B, Shigeto T, and Mizunuma H (2011). *Combination of ciglitazone, a peroxisome proliferator-activated receptor gamma ligand, and cisplatin enhances the inhibition of growth of human ovarian cancers. J Cancer Res Clin Oncol* **137**(8), 1219–1228. http://dx.doi.org/10.1007/s00432-011-0993-1 [Epub 2011/06/18. PubMed PMID: 21681689].

[48] Sterba J, Valik D, Mudry P, Kepak T, Pavelka Z, Bajciova V, Zitterbart K, Kadlecova V, and Mazanek P (2006). *Combined biodifferentiating and antiangiogenic oral metronomic therapy is feasible and effective in relapsed solid tumors in children: single-center pilot study. Onkologie* **29**(7), 308–313. http://dx.doi.org/10.1159/000093474 [PubMed PMID: 16874014].

[49] Zapletalova D, Andre N, Deak L, Kyr M, Bajciova V, Mudry P, Dubska L, Demlova R, Pavelka Z, and Zitterbart K, et al (2012). *Metronomic chemotherapy with the COMBAT regimen in advanced pediatric malignancies: a multicenter experience. Oncology* **82**(5), 249–260. http://dx.doi.org/10.1159/000336483 [PubMed PMID: 22538363].

[50] Araki H, Tamada Y, Imoto S, Dunmore B, Sanders D, Humphrey S, Nagasaki M, Doi A, Nakanishi Y, and Yasuda K, et al (2009). *Analysis of PPARalpha-dependent and PPARalpha-independent transcript regulation following fenofibrate treatment of human endothelial cells. Angiogenesis* **12**(3), 221–229. http://dx.doi.org/10.1007/s10456-009-9142-8 [Epub 2009/04/10. PubMed PMID: 19357976].

[51] Gamerdinger M, Clement AB, and Behl C (2007). *Cholesterol-like effects of selective COX inhibitors and fibrates on cellular membranes and amyloid-{beta} production. Mol Pharmacol* **72**(1), 141–151. http://dx.doi.org/10.1124/mol.107.034009 [PubMed PMID: 17395689].

[52] Nadanaciva S, Dykens JA, Bernal A, Capaldi RA, and Will Y (2007). *Mitochondrial impairment by PPAR agonists and statins identified via immunocaptured OXPHOS complex activities and respiration*. *Toxicol Appl Pharmacol* **223** (3), 277–287 [Epub 2007/07/31. doi: S0041-008X(07)00265-7 [pii] 10.1016/j.taap.2007.06.003. PubMed PMID: 17658574].

[53] Zungu M, Felix R, and Essop MF (2006). *Wy-14,643 and fenofibrate inhibit mitochondrial respiration in isolated rat cardiac mitochondria*. *Mitochondrion* **6**(6), 315–322 [Epub 2006/10/19. doi: S1567-7249(06)00175-9 [pii] 10.1016/j.mito.2006.09.001. PubMed PMID: 17046337].

[54] Carlson BL, Pokorny JL, Schroeder MA, and Sarkaria JN (2011). *Establishment, maintenance and in vitro and in vivo applications of primary human glioblastoma multiforme (GBM) xenograft models for translational biology studies and drug discovery*. *Curr Protoc Pharmacol*. http://dx.doi.org/10.1002/0471141755.ph1416s52 [Chapter 14:Unit 14 6. PubMed PMID: 21743824; PMCID: 3129784].